ACSNANO

www.acsnano.org

ARTICLE

Typhaneoside-Tetrahedral Framework Nucleic Acids System: Mitochondrial Recovery and Antioxidation for Acute Kidney Injury treatment

Ran Yan, Weitong Cui, Wenjuan Ma, Jiajie Li, Zhiqiang Liu, and Yunfeng Lin*

Cite This: *ACS Nano* 2023, 17, 8767–8781

Read Online

ACCESS | Metrics & More | Article Recommendations | Supporting Information

ABSTRACT: **Acute kidney injury (AKI) is not only a worldwide problem with a cruel hospital mortality rate but also an independent risk factor for chronic kidney disease and a promoting factor for its progression. Despite supportive therapeutic measures, there is no effective treatment for AKI. This study employs tetrahedral framework nucleic acid (tFNA) as a vehicle and combines typhaneoside (Typ) to develop the tFNA-Typ complex (TTC) for treating AKI. With the precise targeting ability on mitochondria and renal tubule, increased antiapoptotic and antioxidative effect, and promoted mitochondria and kidney function restoration, the TTC represents a promising nanomedicine for AKI treatment. Overall, this study has developed a dual-targeted nanoparticle with enhanced therapeutic effects on AKI and could have critical clinical applications in the future.**

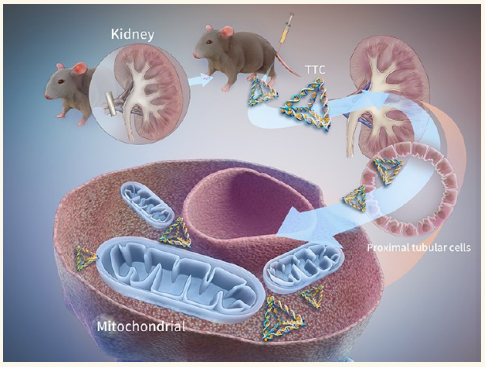

KEYWORDS: *acute kidney injury, tetrahedral framework nucleic acid, typhaneosides, mitochondria, oxidative stress*

Acute kidney injury (AKI), a series of syndromes, has similar clinical manifestations but various pathogenic causes, including sepsis, trauma, cardiac surgery, nephrotoxic drugs, *etc.*[1,2] AKI is identified by the increased risk of renal injury, failure, or loss of kidney function and end-stage kidney disease (ESRD) in RIFLE.[3] According to the Acute Kidney Injury Network (AKIN) criteria, AKI is diagnosed with one of the following criteria: (i) serum creatinine (Scr) increasing by 0.3 mg/dL in 48 h; (ii) 1.5 times of baseline in 7 days; (iii) urine volume <0.5 mL/kg/h for 6 h.[1] AKI is a severe global problem across regions,[4] occurring in 20% of the hospitalized patients and almost half of the patients in the intensive-care unit (ICU).[5−7] Patients with AKI have a higher mortality rate, typically 10% 20% in hospitalized patients and 44.7%∼53% in ICU patients.[2,6,7] Even a minor issue in kidney function could cause an adverse prognosis and affect AKI long-term outcomes,[8] and approximately 6% of patients identified with AKI developed into ESRD within 2 years.[9] Furthermore, AKI patients with pre-CKD had 28 times more risk of progressing to stage 4 CKD than patients without AKI,[10] indicating that AKI is a risk factor for dependent CKD and a promoter factor for its progression.[10,11] In 2013, the International Society of Nephrology (ISN) announced a worldwide object, "0by25"-no patient dies from preventable or untreated AKI by 2025.[4,12] However, at present, the primary clinical treatment for AKI is still supportive therapy; there is neither non-nephrotoxic treatment available to cure early phase AKI nor effective management to improve disease outcomes, which are in urgent need.[13]

AKI arises from various causes and frequently evolves into a secondary injury known as ischemia-reperfusion (I/R) injury.[2,14−16] Second only to the brain, the kidney owns the most abundant mitochondria, especially in proximal tubule cells, which undertake approximately 70% of glomerular filtration and solute reabsorption.[14] The I/R injury causes renal mitochondrial dysfunction, metabolism disorder, and subsequent impaired renal function.[17,18] The inner mitochondrial membrane (IMM) of mitochondria contains complex I∼IV, also known as the electron transport chain (ETC), which drives adenosine triphosphate (ATP) production.[18] In physiological conditions, ETC (mostly complexes I and III)

Received: March 6, 2023
Accepted: April 12, 2023
Published: April 14, 2023

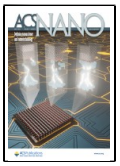

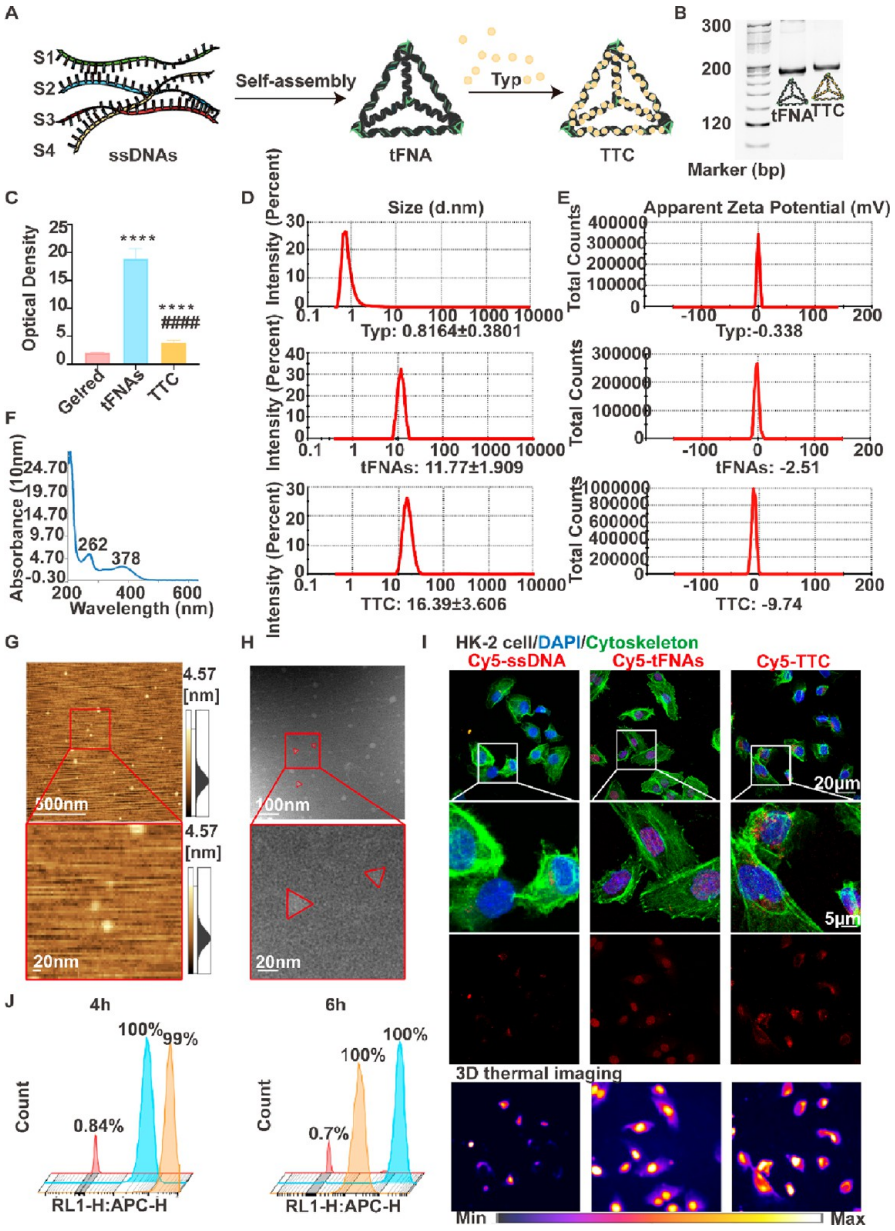

Figure 1. Characterization and biocompatibility of TTC. (A) Schematic diagram of the production of tFNAs and TTCs. (B) tFNA and TTC pictures on PAGE. (C) Fluorescence emission spectra of Gel-Red (λex = 312 nm) in the presence of tFNAs (250 nM) or TTC (tFNA-Typ: 250 nM−50 μM). Statistical analysis: ****p < 0.0001 vs Gel-Red, ####p < 0.0001 vs tFNAs (n = 5). (D) Sizes of Typ, tFNAs, and TTC are 2.4170 ± 0.1417, 11.77 ± 1.909, and 16.93 ± 3.727 nm, respectively. ζ-potentials are −0.338 ± 2.28, −2.51 ± 3.7, and −9.74 ± 3.71 mV. (F) Absorption peaks of TTC (tFNAs ∼ 262 nm, Typ ∼378 nm). (G) AFM images of TTC. (H) TEM images of TTC. (I) The uptake of TTC by HK-2 after 6 h. red, TTC; blue, nuclei; green, cytoskeleton. (J) Flow cytometry to see the uptake of tFNAs and TTC by HK-2 after 4 and 6 h. Blue, tFNAs; orange, TTC.

generates adequate reactive oxygen species (ROS)[19] to participate in the signal channel and is managed by superoxidase dismutase (SOD).[18,20] However, under I/R injury conditions, redundant ROS formation exceeds the oxidative capacity of mitochondria. Accumulated ROS increases the penetrability of the outer mitochondrial membrane (OMM), and the free pro-apoptotic factor cytochrome c (Cyto C) is released from mitochondria to the cytoplasm and activates Caspase, leading to cell apoptosis. Furthermore, mitochondrial fragmentation resulting from a fission and fusion imbalance is also a potential source of ROS.[17] Eventually, proximal tubule epithelial cell apoptosis combined with metabolic disorder and ATP depletion lead to tubular failure and urine−blood barrier damage and eventually result in the declined glomerular filtration rate (GFR) and renal dysfunction. Moreover, constant incomplete recovery of mitochondrial and renal function leads to CKD.[18,21]

In traditional Chinese medicine, the pollen of the genus *Typha angustifolia* L. (Typhaceae), known as "Pu Huang," is an aquatic plant with widespread distributions.[22] Typhaceae, as a major active herb of the formula,[23] has an active effect on early phase renal injuries, including AKI, of which the flavonoid ingredient typhaneoside (Typ), (isorhamnetin-3-*O*-[2G-α-L-rhamnopyranosyl]-α-L-rhamnopyranosyl-[1−6]-β-D-glucopyranoside),[24] is the primary extract.[25−28] Typ possesses a sound biological and antioxidative effect.[22,29] However, the under-

https://doi.org/10.1021/acsnano.3c02102
ACS Nano 2023, 17, 8767−8781

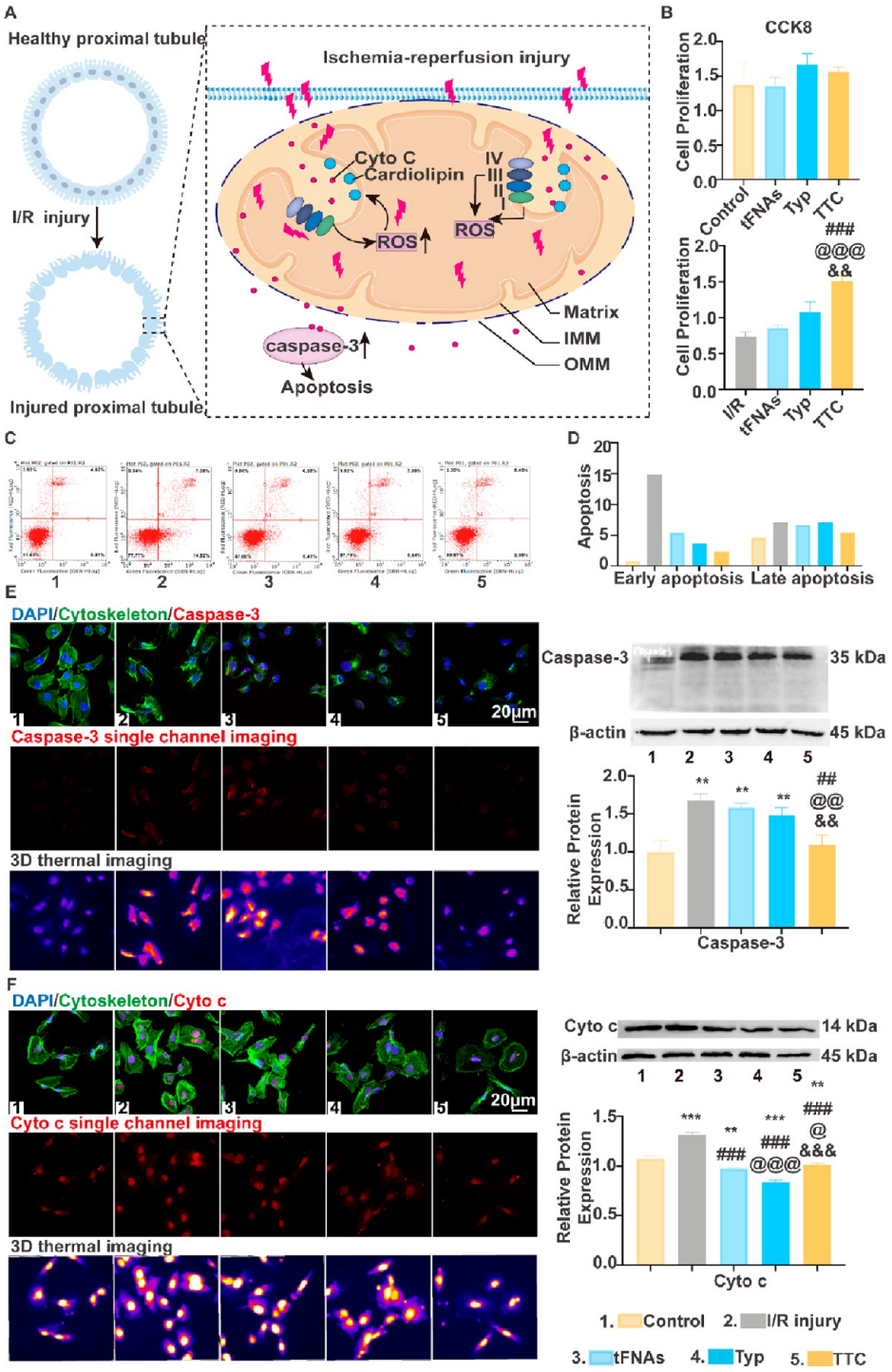

Figure 2. TTC decreased cell apoptosis after I/R Injury. (A) Schematic graph of I/R injured tubular cells. (B) Cell viability of tFNAs, Typ, and TTC on healthy and I/R HK-2 cells analyzed by CCK-8 assay (n = 3). (C) Cell apoptosis in five groups: the control group, I/R group, I/R+tFNAs group, I/R+Typ group, and the I/R+TTC group using flow cytometry. (D) Quantification of (C), including early and late apoptosis rate of cells. (E) Expression of Cyto C in HK-2 after tFNAs, Typ, and TTC treatment using confocal microscope and Western blot. Quantification of related proteins calculated by ImageJ (n = 3). (F) Expression of Caspase-3 in HK-2 after tFNAs, Typ, and TTC treatment using confocal microscopy and Western blot. Quantification of related proteins calculated by ImageJ (n = 3). The statistics are presented as mean ± standard deviation. Statistical analysis: *p < 0.05, **p < 0.01, ***p < 0.001 (Groups: *, control; #, I/R; @, tFNAs; &, Typ).

lying potential pharmacological mechanisms of Typ in AKI are rarely studied. Similar to most traditional Chinese medicine monomers,[30,31] Typ is of limited therapeutic use because of its instant degradation, poor water-solubility, and meager systemic bioavailability.[32−34] Therefore, optimized properties of Typ in AKI therapy are in great necessity.

DNA nanostructures, characterized by their natural biocompatibility, stable structure, and high bioavailability, have recently become a heated research topic.[35,36] Among them, tetrahedral framework nucleic acids (tFNAs), which are formed by four single-strand DNAs (ssDNAs) *via* one-pot annealing,[37] are easily prepared and highly stable for extensive

https://doi.org/10.1021/acsnano.3c02102
ACS Nano 2023, 17, 8767−8781

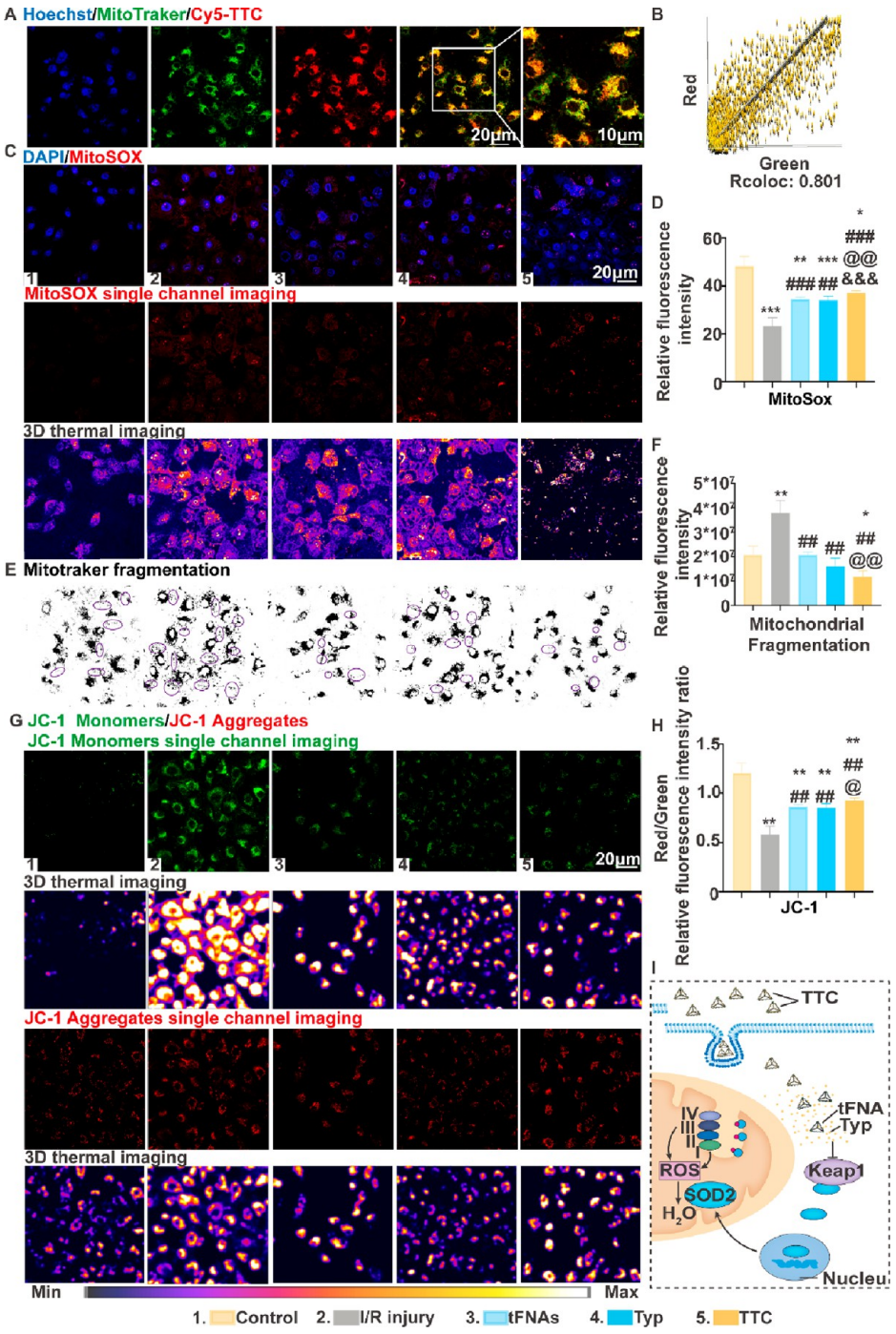

Figure 3. TTC recovered mitochondrial function after I/R Injury. (A) Colocalization of mitochondria and TTC was observed by confocal microscopy. Red, TTC; blue, nuclei; green, cytoskeleton. (B) Colocalization analysis of (A), the Rcoloc is 0.801. (C) Mitochondrial ROS (mtROS) production in five groups: the control group, I/R group, I/R+tFNAs group, I/R+Typ group, and the I/R+TTC group. Red, MitoSOX; blue, nuclei; green, cytoskeleton. (D) Quantification of (C): relative fluorescence intensity of MitoSOX (n = 5). (E) Mitochondrial morphology in five groups and the fragmentation of mitochondria is circled by purple ellipses. (F) Quantification of (E): relative fluorescence intensity in regions circled (n = 5). (G) MMP in five groups. Red fluorescence, JC-1 aggregates; green fluorescence, JC-1 monomers. (H) Quantification of (G): the intensity ratio of red/green fluorescence in five groups (n = 5). (I) Schematic graph of TTC effect on I/R injured tubular cells. Data are presented as mean ± SD. Statistical analysis: *p < 0.05, **p < 0.01, ***p < 0.001 (Groups: *, control; #, I/R; @, tFNAs; &, Typ).

applications.[38,39] TFNAs can also be used as a delivery system, and the drug loading mechanisms include electrostatic interaction, hybridization,[40,41] and groove docking.[42] It has been illustrated that tFNAs can load traditional Chinese medicine monomers such as curcumin by encapsulating small-molecule drugs onto duplex DNA structures.[34,37] Furthermore, based on a negative surface charge on the tetrahedral frame, tFNAs exhibit smooth endocytosis *via* the caveolin-mediated pathway[43,44] to facilitate the intracellular accumulation of drugs carried by tFNAs.[45] Moreover, a previous study has demonstrated that tFNAs have low nephrotoxicity and enhanced antioxidative efficacy through scavenging reactive

https://doi.org/10.1021/acsnano.3c02102
ACS Nano 2023, 17, 8767−8781

oxygen species (ROS).[46] This study employed tFNAs and Typ to develop a tFNA-Typ complex (TTC), which could desirably optimize the bioavailability and stability of Typ to alleviate mitochondrial oxidative stress and achieve mitochondrial function recovery. As a result, a decrease in cell apoptosis is expected to alleviate kidney injury and improve AKI outcomes.

RESULTS

Characterization and Biocompatibility of TTC. Previous studies have confirmed that small molecules could bind to tFNAs *via* a groove docking mechanism.[37] In this study, tFNAs, designed as the transport vehicle, were assembled by four ssDNA first (Table S1). Next, the Typ was encapsulated into tFNAs to form a stable complex (TTC) (Figure 1A). The polyacrylamide gel electrophoresis (PAGE) results (Figure 1B) showed the molecular position of tFNAs, owing to the heavier molecular weight of TTC, the position of TTC in the PAGE images was slightly higher than that of tFNAs, indicating the successful synthesis. Typ is embedded onto the double helix groove regions of DNA, similar to nucleic acid detector molecule GelRed.[47] We, respectively, stained tFNAs and TTC with GelRed and measured the fluorescence spectra. The fluorescence intensity of the TTC was lower than that of tFNAs (Figure 1C) and GelRed alone, further verifying the successful interaction between tFNAs and Typ. Then, the size and ζ-potential were detected with dynamic light scattering (DLS). Typ, tFNAs, and TTC hydrodynamic sizes were 2.4170 ± 0.1417, 11.77 ± 1.909, and 16.93 ± 3.727 nm, respectively (Figure 2D). The ζ-potentials of all nanoparticles were −0.338 ± 2.28, −2.51 ± 3.7, and −9.74 ± 3.71 mV, respectively (Figure 2E). Moreover, the UV−vis absorption of TTC (Figure 1F) contained the characteristic absorption peak of tFNAs (~260 nm) and the characteristic absorption peak of Typ (~378 nm). Atomic force microscopy (AFM) and transmission electron microscopy (TEM) were operated to characterize nanoparticles. AFM and TEM images showed that TTC occupied nearly 20 nm (Figure 1G,H). These results confirm the successful synthesis of TTC, showing that tFNAs could embed Typ into helix structures and the tFNAs might be a potential carrier system for traditional Chinese medicines and similar bioactive molecules.

Besides, we detected the encapsulation efficiency (EE) and loading efficiency (LE) of Typ into tFNAs in different w/w ratios (Figure S1). As encapsulation efficiency declined, the loading efficiency raised. The point of intersection is the most appropriate, where the concentration of Typ is 50 μM, the EE reached ≈50% and the LE of the nanosystem was ≈34%. In subsequent experiments, the corresponding ratio (250 nM tFNAs/50 μM Typ) was employed.

Previous studies[48,49] have confirmed that tFNAs could protect loaded molecules from the degradation of the enzymes to enhance the stability of small bioactive particles. To further confirm the drug stability, tFNAs and TTC were incubated with 10% fetal bovine serum (FBS) at 37° and detected by PAGE. As illustrated in Figure S2, approximately 80% tFNAs and TTC still existed after 4 h and 40% lasted to 12 h, demonstrating the quality stability of tFNAs and TTC.

To verify the cellular uptake of tFNAs and TTC, the human kidney-2 (HK-2) cells were incubated with cyanine dye 5 (Cy5)-loaded ssDNA, Cy5-loaded tFNAs, or Cy5-loaded TTC for 4 or 6 h and then measured with a confocal microscope and flow cytometer (Figure 1I,J). According to the confocal image result (Figure 1I), many tFNAs and TTC could penetrate the cell membrane at 4 and 6 h, in agreement with the flow cytometry results (Figure 1J). Both results demonstrated that Typ did not interfere with the internalization of tFNAs.

TTC Decreased Cell Apoptosis after I/R Injury. The schematic graph of the process of apoptosis in I/R injured tubular cells is shown in Figure 2A. I/R is the most common secondary event in AKI, and the proximal tubule is most sensitive to I/R. Therefore, HK-2 cells were selected to build an I/R injury model *in vitro*. To assess the modeling time and conditions, a Cell Counting Kit-8 (CCK8) assay was adopted. We selected 6 h of hypoxia followed by 24 h of reoxygenation to achieve a 50% decrease in cell viability in the modeling group, which was also the model adopted in subsequent experiments. Then, we assessed the cell viability of tFNAs, Typ, or TTC at different concentrations. In the tFNAs group, 250 nM tFNAs has the steadiest promoting effect on cell viability (Figure S3A). In the TTC group, the tFNAs/Typ ratio of 250 nM/50 μM (the drug/carrier ratio was utilized in the following experiments if not specified) had the soundest effect on promoting the cell viability, which was consistent with the results of EE and LE (Figure S1). Finally, we compared the effects of TFNAs (250 nM), Typ (50 μM), or TTC (250 nM/50 μM) on the proliferation of healthy and I/R injury cells (Figure 2B), which showed that none of tFNAs, Typ, nor TTC had cytotoxicity in healthy cells, and the I/R injury cell viability in the TTC group was significantly higher compared to that in the tFNAs and Typ groups.

To detect the antiapoptotic effect of TTC, we evaluated cell apoptosis in five groups: the control group, I/R group, I/R +tFNAs, I/R+Typ, and I/R+TTC groups using flow cytometry. As shown in Figure 2C,D, TTC reduced the early and late apoptosis ratio. These results signified that TTC could prevent I/R-treated cells from apoptosis, confirming the curative effect of TTC on AKI in the cell model. Next, to validate the underlying pathway, we identified the protein expression of Cyto C and Caspase-3, and the results (Figure 2E,F) demonstrated that TTC significantly inhibited the protein expression of Cyto C and Caspase-3, which implies that the escaped Cyto C might activate Caspase-3, contributing to cell apoptosis.

TTC Recovered Mitochondrial Function after I/R Injury. We hypothesized that the underlying mechanism of TTC in cell regulation was related to its action on mitochondria. To verify this hypothesis, the mitochondrial targeting ability of TTC was first investigated. We incubated Cy5-loaded tFNAs and Cy5-loaded TTC with HK-2 cells and stained mitochondria with a Mito-Tracker Green probe. As shown in Figure 3A, red fluorescence (tFNAs/TTC) mostly overlapped with green fluorescence (Mito-Tracker). The scatterplot analysis of fluorescence colocalization shows that almost all the data points fell on a straight diagonal line, and the rcoloc meaning is 0.801, which means there is a strong correlation between TTC and mitochondria (Figure 3B). These results suggested that tFNAs and TTC both own mitochondrial targeting ability, which is the basis for the following effects on mitochondria.

Excessive ROS could release pro-apoptotic factor Cyto C from the IMM,[50] and it was shown in the above results that Cyto C was the underlying promoter for cell apoptosis. The capability of tFNAs, Typ, and TTC to depress mitochondrial ROS (mtROS) generation in model HK-2 cells was probed through a mtROS sensor (MitoSOX). The relative fluorescence intensity of mtROS in confocal laser microscopy images

https://doi.org/10.1021/acsnano.3c02102
ACS Nano 2023, 17, 8767−8781

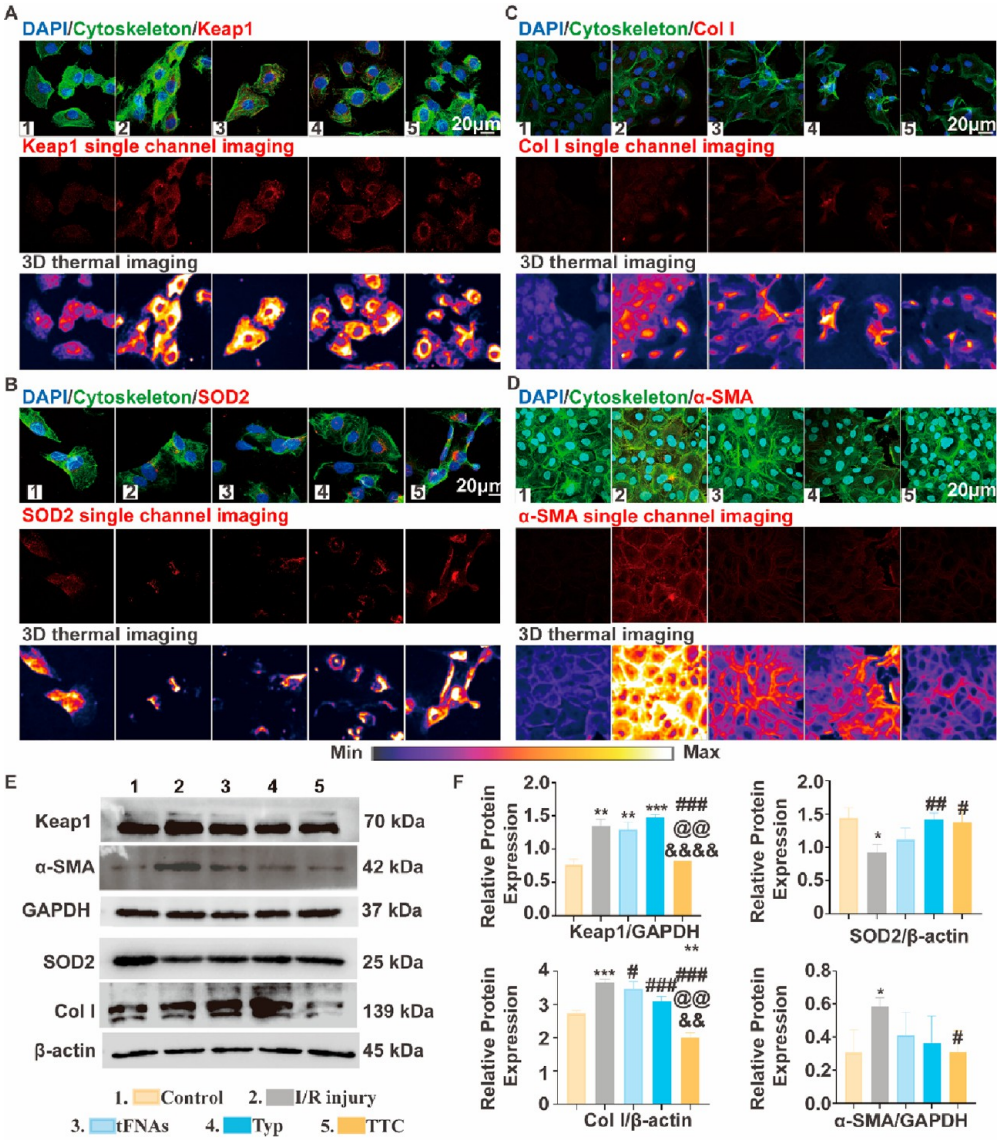

Figure 4. TTC reduced mitochondrial oxidative stress through Keap1/SOD2 signaling and fibrotic progress after I/R injury. (A) IF confocal microscope of Keap1. Red, Keap1; blue, nuclei; green, cytoskeleton. (B) IF confocal microscope of SOD2. Red, SOD2; blue, nuclei; green, cytoskeleton. (C) IF confocal microscope of Col I. Red, Col I; blue, nuclei; green, cytoskeleton. (D) IF confocal microscope of α-SMA. Red, α-SMA; Blue, nuclei; Green, cytoskeleton. (E) Protein expression of Western blot analysis of Keap1/SOD2/Col I/α-SMA. (F) Quantification of related proteins calculated by ImageJ (n = 3). Data are presented as mean ± SD. Statistical analysis: *p < 0.05, **p < 0.01, ***p < 0.001 (Groups: *, control; #, I/R; @, tFNAs; &, Typ).

extensively increased after I/R injury (Figure 3C,D); however, TTC markedly decreased the mtROS level compared with tFNAs and Typ. The result implied that TTC could hinder mtROS production.

Imbalance in mitochondrial dynamics has harmful effects on mitochondrial homeostasis,[18,51] which is a potential source of ROS. Fission and fusion processes constantly take place to maintain mitochondrial morphology and meet cellular energy requirements.[21] In the case of fission, mitochondria split into two or more to acquire more ATP,[52] whereas fusion combines two or more mitochondria that can complement fission.[18] Under oxidative conditions, fusion decreases while fission increases to defend against damaged metabolites; as a result, the imbalance between fission and fusion contributes to mitochondrial fragmentation. We used the Mito-Tracker Green probe to stain mitochondria to observe mitochondrial morphology in the five groups. The images (Figure 3E) and quantification (Figure 3F) showed that the fragmentation of mitochondria (circled by purple ellipses) was less after TTC treatment, which proved the function of TTC in recovering the dynamics of mitochondria.

The mitochondrial membrane potential (MMP) is intimately correlated with mitochondrial dynamics.[14,53] The fluorescent probe 5,5,6,6′-tetrachloro-1,1′,3,3′-tetraethyl-imidacarbocyanine iodide (JC-1) was applied to evaluate MMP. With the increasing MMP, JC-1 accumulates in the mitochondrial matrix, producing red fluorescence. In contrast, the JC-I monomer could not accumulate in low MMP, producing green fluorescence. Thus, the red/green fluorescence intensity rate indicates MMP and the degree of mitochondrial polarization. Results shown in Figure 3G,H indicated that the red/green fluorescence intensity ratio was enhanced by TTC, validating that TTC could stabilize the MMP and diminish mitochondrial polarization. The above

https://doi.org/10.1021/acsnano.3c02102
ACS Nano 2023, 17, 8767−8781

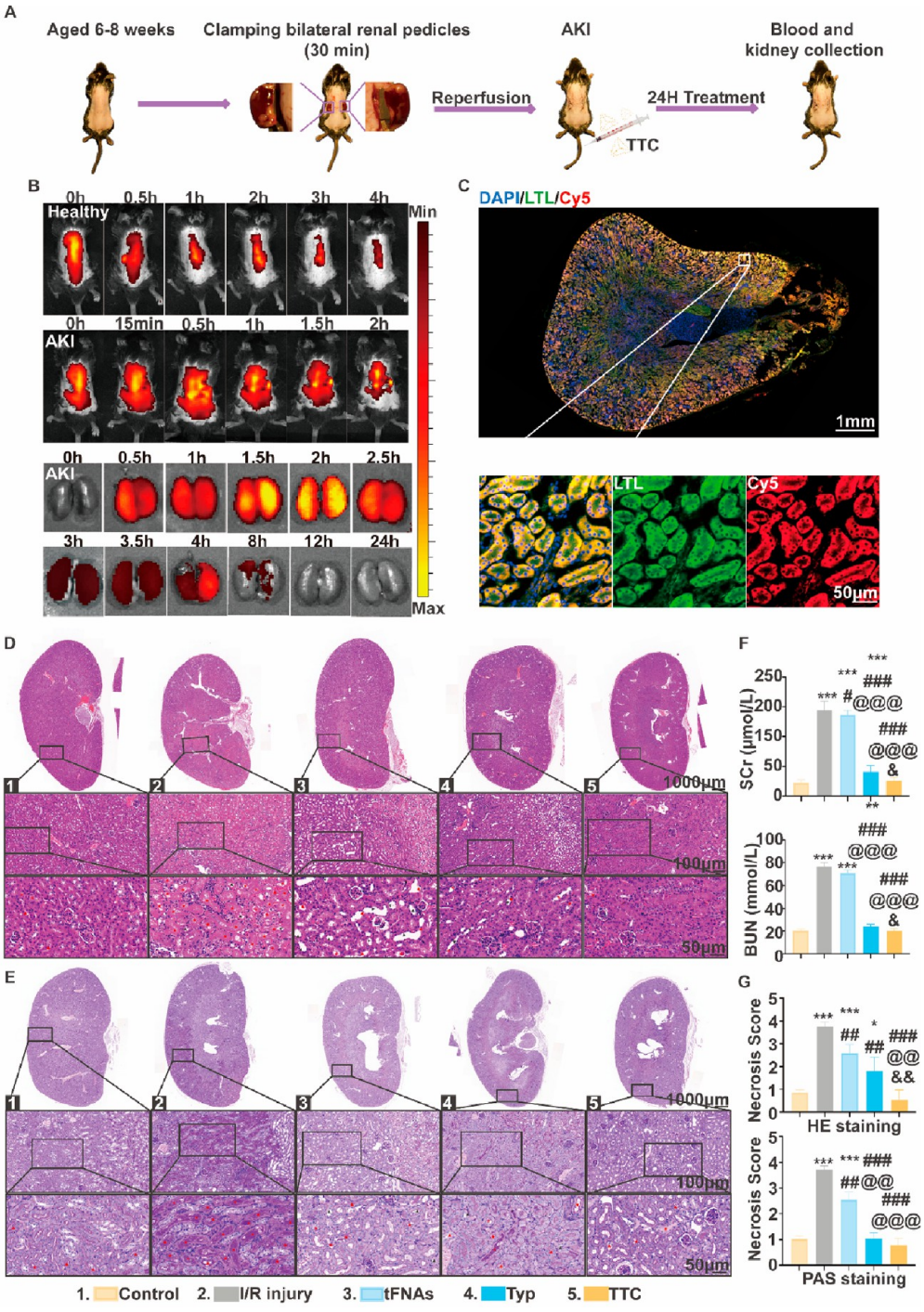

Figure 5. TTC recovered renal function and targeted tubular injury after AKI. (A) Schematic graph of the establishment of murine I/R injured AKI model. (B) TTC biodistribution TTC in healthy and AKI mice and the TTC biodistribution in harvested kidneys from AKI mice. (C) TTC's renal tubular targeting capability Green, renal tubules (LTL); red, Cy5-TTC; blue, nuclei. (D and E) AKI histopathological damage was evaluated by periodic acid−Schiff (PAS) staining and hematoxylin and eosin (H&E) staining. Black arrowheads, brush border loss; red arrowheads, cells slough; red asterisks, hyaline casts. (F) Serum BUN and Scr levels of mice in five groups: the Sham group, AKI +saline group, AKI+tFNAs group, AKI+Typ group, and the AKI+TTC group. (G) The tubular injury score was evaluated according to the percentage of damaged tubules; 10 random tissue sections per mouse have been assessed on H&E or PAS staining. Results were averaged for each mouse (n = 5). Data are presented as mean ± SD. Statistical analysis: *p < 0.05, **p < 0.01, ***p < 0.001 (Groups: *, Sham; #, AKI +saline; @, AKI+tFNAs; &, AKI+Typ).

data suggested that TTC could precisely target mitochondria, maintain mitochondrial morphology, recover mitochondrial dynamics, and reduce mitochondrial ROS, which might be the underlying mechanism of TTC, and the schematic graph of the TTC effect is shown in Figure 3I.

TTC Reduced Mitochondrial ROS through Keap1/SOD2 Signaling and Inhibited Fibrotic Progress. The effect of drugs on ROS was calculated by evaluating protein expression levels of important antioxidant enzymes SOD2 in the mitochondrial inner membrane and adverse regulatory

https://doi.org/10.1021/acsnano.3c02102
ACS Nano 2023, 17, 8767−8781

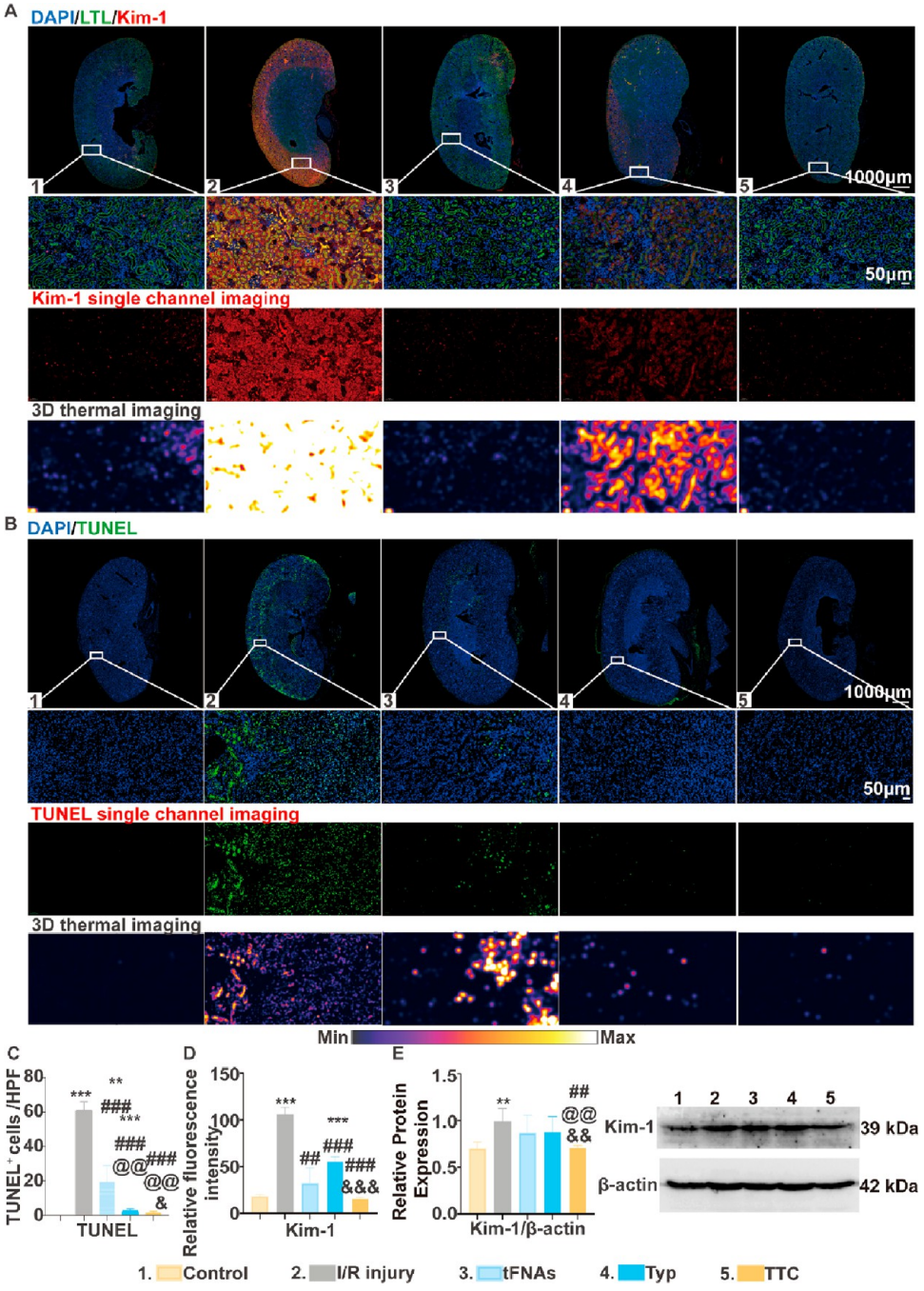

Figure 6. TTC reduced renal injury and apoptosis after AKI. (A) Injured tubules stained with Kim-1. Red, Kim-1; green, renal tubules (LTL); blue, nuclei. (B) TUNEL assay of the apoptotic cells in five groups: the Sham group, AKI+saline group, AKI+tFNAs group, AKI+Typ group, and the AKI+TTC group. Green, TUNEL; blue, nuclei. (C) Quantification of the percentage of TUNEL$^+$ apoptotic cells (n = 5). HPF, High power field (400X). (D) Quantification of (A): relative fluorescence intensity of Kim-1 (n = 5). (E) Protein expression of Western blot analysis of Kim-1. Quantification of related proteins calculated by ImageJ (n = 3). Data are presented as mean ± SD. Statistical analysis: *p < 0.05, **p < 0.01, ***p < 0.001 (Groups: *, Sham; #, AKI+saline; @, AKI+tFNAs; &, AKI+Typ).

factor Kelch-like ECH-associated protein 1 (Keap1) in Western blotting and immunofluorescence staining. As expected, the expression of Keap1 was increased after I/R injury and significantly decreased after TTC treatment (Figure 4A,F,G). Keap1 is an oxidative stress sensor; when it is depleted, ROS falls sharply.[50] SOD2 expression was upregulated after treatment with TTC (Figure 4B,C,F,G), suggesting that TTC could activate the Keap1 depletion and SOD2 augmentation to act as an antioxidant.[21]

Previous studies have reported that mitochondrial dysfunction and ATP reduction are intently relevant to CKD development and progression.[14,18,19,21,54,55] Incomplete recovery after AKI results in renal fibrosis, the pathological accumulation of extracellular matrix (ECM) proteins, mainly collagens in the kidney.[56,57] We then explored the protein levels of α-smooth muscle actin (α-SMA) and collagen I (Col I) by Western blotting and immunofluorescence staining (Figure 4D,E,F,G). The expression levels of α-SMA and Col I were greatly increased after I/R injury but were significantly

https://doi.org/10.1021/acsnano.3c02102
ACS Nano 2023, 17, 8767−8781

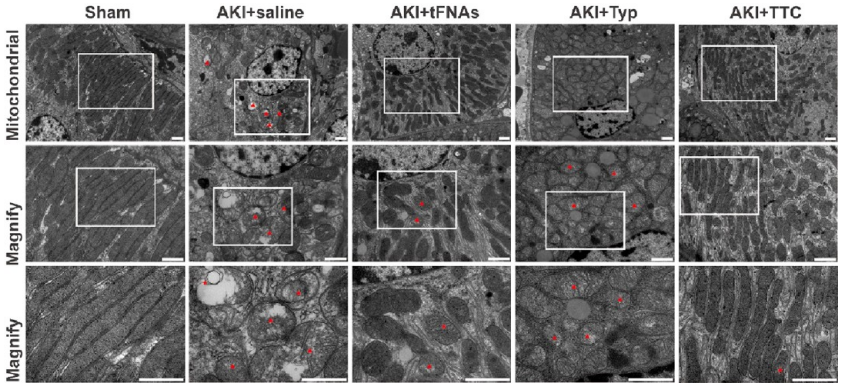

Figure 7. TTC protected mitochondria from damage in AKI mice. Representative TEM image of mitochondria in the renal section. Red arrowheads: mitochondrial swelling with cristae architecture disruption. Red asterisks: mitochondria with membrane breakdown and matrix material leakage into the cytoplasm. Scale bar, 1 μm.

decreased after I/R injured cells were incubated with tFNAs, Typ, and TTC. The expression levels of α-SMA and Col I in TTC-treated cells were substantially lower than those in other groups, which demonstrated that TTC owned strong antifibrotic potential and suggested that TTC might inhibit the progression of AKI to CKD.

Treatment of AKI. An I/R injured AKI animal model was established to study the therapeutic efficiency of TTC *in vivo*. We selected 6−8 weeks male C57 mice, separated both kidneys, and clamped the bilateral kidney pedicle for 30 min to induce ischemia. Saline, tFNAs, Typ, or TTC was administered intravenously after reperfusion, and kidneys were harvested after 24 h (Figure 5A).

Kidney targeting ability is the basis for AKI treatment. Cy5-labeled TTC was injected intravenously and detected by the *in vivo* imaging system (IVIS) Spectrum (PerkinElmer) to access the biodistribution of TTC in healthy and AKI mice. Fluorescence distribution was mainly in the liver and kidneys in the AKI group, and fluorescence was significantly increased and sustained compared to the healthy group, shown in Figure 5B, indicating that TTC was rapidly eliminated by the healthy kidney but preserved in the AKI kidney. Harvested AKI kidneys showed that the fluorescence of TTC peaked at 2 h after TTC administration and still emerged after 4 h (Figure 5B and Figure S4). To observe the biodistribution of TTC at the cellular level, renal tubules on the renal sections were labeled by Lotus-tetragonolobus Lectin (LTL) and TTC with Cy5. The fluorescence of Cy5 and LTL highly overlapped (Figure 5C), proving the renal tubular targeting capability of TTC. The renal tubular damage induces tubular dysfunction and GFR decline, compromising renal functions. Thus, the accurate biodistribution in renal tubules indicates that TTC could be a precise solution for AKI. We also detected the plasma pharmacokinetics of tFNAs and TTC, which showed that the tFNAs and TTC accumulated in the blood for around 2 h after administration. Afterward, we speculated that tFNAs and TTC were distributed into kidneys until kidney clearance (Figure S4).

To access the therapeutic effect of TTC, I/R injured AKI model mice were divided into four groups and, respectively, injected with saline, tFNAs, Typ, and TTC. After 24 h, blood serum was collected, and kidneys were harvested. AKI histopathological damage was evaluated by staining with periodic acid Schiff (PAS) and hematoxylin and eosin (H&E) (Figure 5D,E). The Sham group showed normal renal structure; however, the renal tubular injury was detected in the AKI group by loss of brush borders, hyaline casts formation, and sloughed cells. The focal injury was marked in both tFNAs- and Typ-treated groups, whereas TTC declined tubular damage considerably, with brush borders well-preserved. To quantify tubular injury, 10 randomly selected fields were evaluated on H&E or PAS staining, and a semiquantitatively grading system was then employed, with 0−4 scores depending on the percentage of injured tubules. Results were calculated for each mouse (Figure 5G). The average tubular injury score rose after I/R injured AKI. After treatment with tFNAs, Typ, and TTC, the scores for the above three groups descended significantly. The most obvious score declination was in the TTC-treated group. Blood serum was detected with clinical indexes, serum creatinine (Scr), and blood urea nitrogen (BUN) (Figure 5F), which were elevated after AKI and significantly decreased in TTC group, showing that TTC could restore kidney function.

The injured tubules were further studied by staining with anti−kidney injury molecular-1 (KIM-1) antibody (Figure 6A), which is characteristically expressed in injured renal tubules; the fluorescence and the quantification of relative fluorescence intensity (Figure 6D) were low in the Sham and TTC-treated groups, consistent with the tubular injury score. Besides, the protein expression of KIM-1 also verified that TTC could reduce tubular injury to the greatest extent compared with other groups (Figure 6E).

Cell apoptosis is caused by oxidative stress brought by I/R in AKI. The terminal deoxynucleotidyl transferase-mediated deoxyuridine triphosphate nick-end labeling (TUNEL) assay was used to identify the apoptotic cells in the kidney tissue slices. According to the staining results and quantitative analysis, apoptotic cells in the AKI group largely accumulated compared with the Sham group. Yet, the TTC group had the relatively lowest percentage of apoptotic cells compared with other treatment groups (Figure 6B,C), demonstrating TTC's antiapoptotic effectiveness *in vivo*.

Transmission electron microscopy (TEM) was applied to observe mitochondrial morphology in renal sections of five groups. As seen in TEM images, I/R injured AKI produced extensive mitochondrial damage in proximal tubular cells, confirmed by mitochondrial swelling, matrix brightening, disorganized and fragmented cristae, mitochondrial membrane disruption, and matrix substance that was released into the cytoplasm (Figure 7). After being treated with tFNAs, Typ,

https://doi.org/10.1021/acsnano.3c02102
ACS Nano 2023, 17, 8767−8781

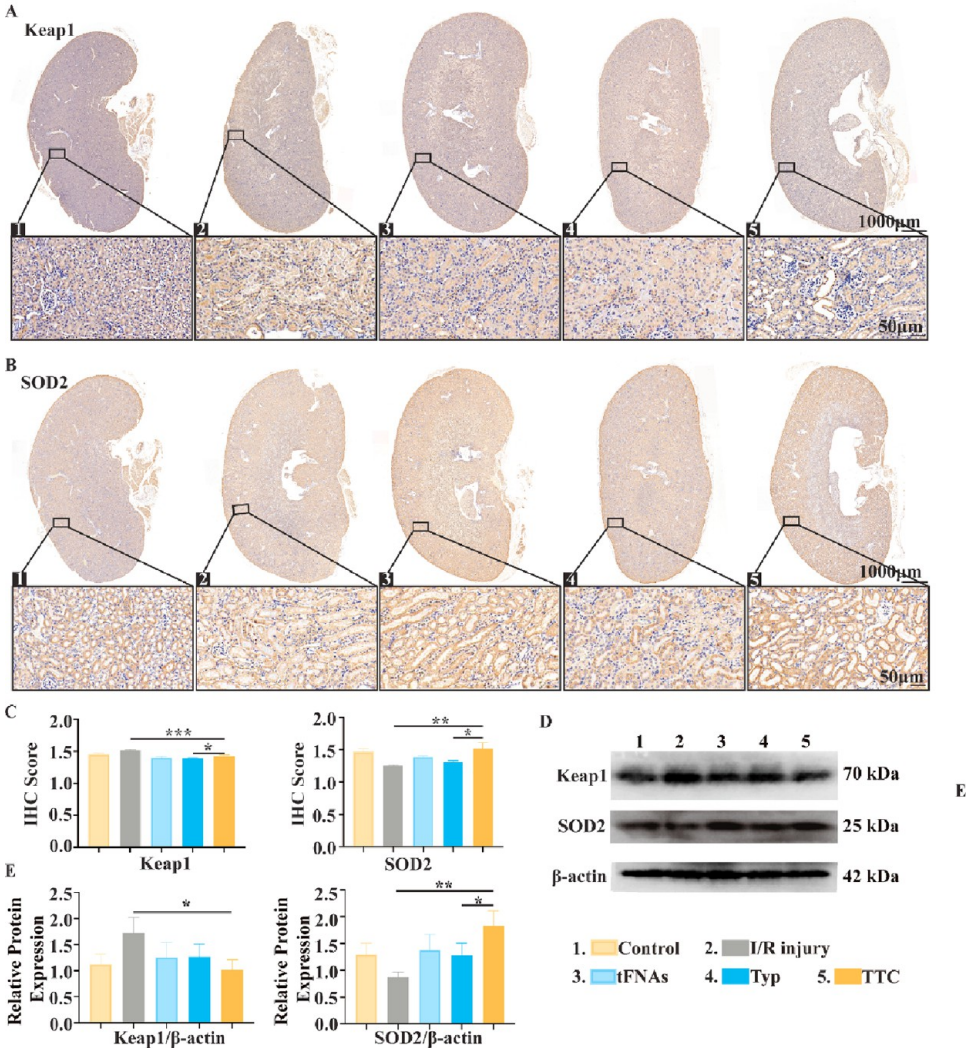

Figure 8. TTC regulated Keap1/SOD2 signaling *in vivo*. (A and B) Keap1 and SOD2 expression in immunohistochemistry analysis. Brown, Keap1/SOD2; blue, nuclei. (C) Quantification of (A and B): IHC score of Keap1 and SOD2 expression (n = 5). (D) Protein expression of Western blot analysis of Keap1 and SOD2. (E) Quantification of related proteins calculated by ImageJ (n = 3). Data are presented as mean ± SD. Statistical analysis: *p < 0.05, **p < 0.01, ***p < 0.001 (Groups: *, Sham; #, AKI+saline; @, AKI+tFNAs; &, AKI+Typ).

and TTC, the number of damaged mitochondria significantly reduced. In contrast, samples from AKI animals treated with TTC revealed fewer damaged mitochondria and a greater proportion of elongated mitochondria with preserved cristae structure.

In agreement with the *in vitro* findings, TTC significantly SOD2 expression and abrogated the expression levels of Keap1 in the injured kidney (Figure 8A–F) in immunohistochemistry analysis and Western blotting analysis, further confirming that TTC could decrease cell apoptosis through antioxidative effect.

The main organs were harvested after drug administration. Heart, spleen, lung, and liver were stained with H&E, but no significant morphological alterations or tissue damage were visible in any groups (Figure S5).

DISCUSSION

In this study, we developed a therapeutic system (tFNA-Typ complex, TTC) for AKI. TTC was found to display excellent endocytosis and precise mitochondrial target ability to recover mitochondria morphology function. Consequently, cell apoptosis was detected to decline both *in vitro* and *in vivo*; besides, the renal injury was decreased and kidney function was restored in ischemia-reperfusion (I/R) injured AKI, verifying the role of TTC in mitochondrial recovery in AKI treatment.

Acute kidney injury is a syndrome with multiple etiologies, including infection,[58,59] ischemia-reperfusion,[59−61] nephrotoxic drugs,[62−64] immune system disorders,[65] and other triggering factors.[66] IRI-induced dysfunctional conditions include kidney transplantation, circulatory arrest,[60,61] hypovolaemic shock,[67] and severe blood loss.[68] In fact, regardless of the cause, AKI often tends to induce a secondary ischemia-reperfusion (I/R) injury due to hemodynamic changes in the kidney.[2,14−16] Paradoxically, it is reperfusion, the basic therapeutic intervention for ischemia, that drives the histopathological changes.[69] The early stage of reperfusion is very important; the changes in tissues will lead to long-term tissue damage and dysfunction.[70] Renal tubular cells that perform most of the glomerular filtration and solute reabsorption are most sensitive to I/R. The consequent apoptosis of renal tubule cells results in tubular failure, obstruction of blood flow structures, and further inhibits glomerular filtration.[15] Our study found that tFNAs own tubular targeting ability, which is consistent with

https://doi.org/10.1021/acsnano.3c02102
ACS Nano 2023, 17, 8767−8781

our previous related research.[46] tFNAs have a tetrahedral framework structure, which makes it easy to enter cells. Moreover, based on the double-stranded structure and chemical properties of DNA, tFNAs can carry various drugs. Our study confirmed that Typ could be embedded in the tFNAs double-stranded structure and transported into cells. Previous studies have shown that Typ has the effect of treating ischemia-reperfusion injury. In addition, tFNAs have also been confirmed to be effective in acute kidney injury. Our approach to building the tFNA-Typ complex has the following advantages: (i) tFNAs could desirably optimize the bioavailability and stability of Typ and (ii) the complex can play a dual effect of tFNAs and Typ on treating the disease.

Previous studies have shown that the first injury after reperfusion is the impairment of mitochondrial structure and function.[71,72] Renal tubules are one of the most metabolically active epitheliums in the human body; therefore, the main site of mitochondrial destruction is in the proximal tubule.[17] Mitochondrial dysfunction leads to metabolic disorder, ROS accumulation, cellular oxidative damage, and subsequent cell apoptosis. Renal tubule cell apoptosis gives rise to irreversible tubular injury and disability of the entire nephron. The nephrons are replaced by fibrous tissue, resulting in permanent impairment of kidney function.[73] Therefore, it is crucial to restore mitochondrial function at an early stage. Our previous preliminary study showed that tFNAs have a therapeutic effect on mitochondrial damage, and we also hypothesized that the targeting effect of tFNAs on renal tubular cells is derived from the targeting of mitochondria. In our study, we confirmed this hypothesis and proved that TTC complexes could repair mitochondria and prevent cell apoptosis by reducing oxidative damage.

In a physiological state, ROS are produced by mitochondria ETC, as a normal metabolic byproduct of oxygen and one that takes an essential part in cell signaling and homeostasis. However, under I/R injury conditions, redundant ROS formation can make the OMM more permeable and release Cyto C, a pro-apoptotic substance produced from mitochondria and activates Caspase to cause excessive cell death.[14] In the mitochondria, SOD2 mainly maintains the homeostasis of redox reactions and controls oxidative stress, which converts ROS to hydrogen peroxide (H_2O_2) and oxygen (O_2).[18] Keap1 is the cellular receptor for oxidative stress; inhibition of Keap1-dependent ubiquitination of Nrf2 correlates with antioxidant reaction.[74,75] In this study, we demonstrated that TTC could downregulate KEAP1 expression and promote the production of SOD2 to regulate ROS in mitochondria and to release mitochondrial damage

Limitations of the Study. In our study, the unexpected outcome of AKI to a great extent contributes to the promotion of CKD. This study explored the expression alteration of the main protein Col I and α-SMA but still lacked long-term observation and proof *in vivo*. Hence it is essential to determine the progress from AKI to CKD and its key points, which could be the therapy target.

Another limitation of our study is that there are other possible mitochondrial signaling pathways and oxidant-neutralizing enzymes that need to be explored, such as the peroxisome proliferator-activated receptor-γ coactivator 1α (PGC1α), the main regulator of mitochondrial biogenesis, and nicotinamide adenine dinucleotide (NAD^+), an important regulator for mitochondrial function.[19] Future research should thus investigate whether our findings may be used to develop a successful treatment.

CONCLUSIONS

Our results show that, embedded in the helix structure of tFNAs, Typ could improve its bioavailability and precisely target mitochondria in renal tubular cells in the kidney. TTC exhibited non-nephrotoxicity and an extraordinary capability in mitochondrial repair and cell apoptosis prevention both *in vitro* and *in vivo*, so as to inhibit renal injury and restore kidney function. Overall, TTC would be a promising treatment for clinical AKI, as well as other mitochondria-related diseases, and provide a DNA-based therapy for AKI.

METHODS

Synthesis of TTC. Four designed assembled ssDNA were added into the TM buffer (50 mM $MgCl_2$ and 10 mM Tris-HCl, pH 8.0) at an equal ratio to formulate tFNAs. Typ (Macklin, Shanghai, China) was dissolved in dimethyl sulfoxide (DMSO) and added to tFNAs to reach the ultimate concentration of Typ (50 μM) and tFNAs (250 nM). Based on previous research, the TTC was combined based on previous research by shaking the mixture for 6 h. The EE and the LE were calculated by measuring the concentration of unloaded Typ, acquired through diafiltration by an 30 Kda ultracentrifuge tube. Typ concentration was confirmed *via* spectral detection at a wavelength of 376 nm using an ultramicrospectrophotometer and the establishment of a standard curve. The specific formulas of the EE and the LE are as follows:

$$\text{encapsulation efficiency of Typ (\%)} = \frac{\text{initial mass of Typ} - \text{residual mass of Typ}}{\text{initial mass of Typ}} \times 100\%$$

$$\text{loading efficiency of Typ (\%)} = \frac{\text{initial mass of Typ} - \text{residual mass of Typ}}{\text{total mass of nanoparticles}} \times 100\%$$

Characterization of tFNAs and TTC. We used GelRed (Varioskan LUX microplate reader, Thermo Scientific), polyacrylamide gel electrophoresis (PAGE), ζ potential and size (Nano ZS, Malvern), TEM (JEM-2100F, JEOL) and AFM (SPM-9700 instrument, Shimadzu, Kyoto, Japan) to verify the successful synthesis of tFNAs and TTC.

Cell Treatment. HK-2 cells were cultured in high glucose Dulbecco's modified eagle medium (DEME) (Corning, NY) containing 10% fetal bovine serum (FBS) (Wisent, Nanjing, China) and 1% penicillin−streptomycin (Hyclone). The I/R group cells were cultured under hypoxia conditions (94% N_2, 5% CO_2, and 1% O_2) in a nutrient-free medium (glucose-free, FBS-free, Gibco) for 6 h, followed by 24 h of reoxygenation in regular medium. The control group cells were incubated in a complete medium in 5% CO_2 and 95% air. Typ, tFNAs, and TTC group cells were incubated with Typ, tFNAs, or TTC after reoxygenation for 24 h

Cell Viability Measurement. The cells seeded in 96-well plates were classified into five groups: the control groups, I/R group, I/R +tFNAs, I/R+Typ, and I/R+TTC group. The Typ, tFNAs, or TTC was added to HK-2 cells to determine the optimal dosage, and the cell viability was detected using a CCK-8 after 24 h of incubation.

Cellular Uptake of TTC. After adherent growth in 6-well plates, the cells were I/R treated, and subsequently, cells were coincubated with Cy5-loaded tFNAs (Cy5-tFNAs, 250 nM) or Cy5-loaded TTC (Cy5-Typ-tFNAs, 50 μM−250 nM) respectively for 6 h. The cells were immobilized in 4% paraformaldehyde after washing with PBS and dyed with 4′,6-diamidino-2-phenylindole (DAPI) and fluorescein isothiocyanate (FITC)-labeled phalloidin. To assess the cellular uptake of tFNAs and TTC, the results were acquired by confocal

https://doi.org/10.1021/acsnano.3c02102
ACS Nano 2023, 17, 8767−8781

microscopy (FV3000, Olympus) and flow cytometer (Attune NxT, Thermo Fisher).

Flow Cytometry. HK-2 cells were plated onto 6-well plates in order to identify cell apoptosis. Following treatment, trypsin digestion and two PBS washes were performed on the cells. A flow cytometer was used to identify cell death after staining the cells with propidium iodide (PI) and Annexin V.

Measurement of Mitochondrial Function. Mitochondrial morphology and mitochondrial targeting were detected using MitoTracker Green (C1048, Beyotime Biotechnology, Shanghai, China). Briefly, HK-2 cells were incubated with MitoTracker staining working solution at 37 °C for 15 min, and the nuclei were stained with Hoechst. Images were acquired by confocal laser microscopy (FV3000, Olympus).

MitoSOX was utilized to detect mitochondrial ROS production in HK-2 cells (M36008, Thermo Fisher). Briefly, MitoSOX (1 mL of 5 μM) was applied to cover cells adhering to the glass-bottom dish at 37 °C for 10 min, and the nuclei were dyed with Hoechst. Images were taken by confocal laser microscopy (FV3000, Olympus).

MMP in HK-2 cells was determined by the JC-1 probe (C2006, Beyotime Biotechnology, Shanghai, China). Briefly,1 mL of JC-1 staining working solution was applied (10 min, 37 °C), and then, cells were rinsed with JC-1 staining buffer. The nuclei were stained with Hoechst, and images were acquired by confocal laser microscopy (FV3000, Olympus). The relative MMP was detected on excitation wavelength of 585/514 nm showing red/green fluorescence.

Animal Model and Treatments. Male C57BL/6 mice (6−8 weeks old) were anesthetized with isoflurane. Mice were randomly divided into five groups: the Sham group, AKI+saline group, AKI +tFNAs group, AKI+Typ group, and the AKI+TTC group. In the AKI mice, the bilateral renal pedicles were clamped to induce renal ischemia until the kidneys' color changed from red to purple. Surgery but without clamps was applied to the Sham group. The mice were kept at a constant body temperature of 37 °C during the entirety of the surgical procedure. Both clamps were unloaded for the kidneys' reperfusion after 30 min. AKI-injured mice were separated into four groups and given intravenously administered saline (100 μL), tFNAs (100 μL, 1 μM), Typ (100 μL, 1.2 mM), or tFNAs-Typ (100 μL, 1 μM−1.2 mM) respectively. After 24 h of treatment, mice in the five groups were euthanized and organs were harvested. And, blood was collected and placed for 30 min at ambient temperature and then centrifuged at 3000 rpm for 15 min to obtain the plasma, detecting BUN and Scr *via* a biochemical automatic analyzer (Vitalab Selectra E).

Bio Distribution of TTC. To assess *in vivo* biodistribution of TTC, Cy5-labeled TTC was injected intravenously into healthy mice and AKI mice. Fluorescence was detected using an IVIS Spectrum (PerkinElmer) every 15 min for 3 h. AKI injured kidneys were separated and imaged every 0.5 h. The plasma was acquired from tail vein every 0.5 h. And, the kidneys with peaked fluorescence were fixed in an OCT embedding medium and frozen, and sections of tissues were incubated with DAPI and LTL staining. Fluorescence images were scanned by a slide scanner (VS200, Olympus).

Kidney Histology and Quantification. The harvested kidneys were fixed with 4% formaldehyde, embedded in paraffin, and sectioned to a thickness of 4 μm. Renal sections were routinely stained with PAS staining and H&E staining reagents, and images were captured using a slide scanner (3DHISTECH, Hungary). Ten random views on H&E or PAS staining were evaluated to count tubular injury scores. The level of tubule impairment was semi-quantitatively evaluated on a 0−4 scale: 0, no lesion; 1, < 25%; 2, 25 to ∼50%; 3, 50 to ∼75%; 4, > 75%, based on the proportion of tubular necrosis shown by brush border loss, hyaline casts, cell sloughing, and tubular dilatation.

TUNEL Assay. Paraffinized renal tissue sections were first dewaxed and then rehydrated. The deparaffinized slices were treated with proteinase K in succession (20 min, room temperature). Afterward, the nuclei were stained with DAPI after being washed three times. The obtained sections were scanned by a slide scanner (3DHISTECH). The relative fluorescence density was measured by ImageJ.

Western Blot. After different treatments, the total protein of HK-2 cells and the kidney tissues in all groups was extracted by lysis buffer. A loading buffer was added to each sample after protein quantification using a NanoPhotometer N60 (Implen). After being boiled for 15 min, samples were isolated on sodium dodecyl sulfate (SDS)-polyacrylamide gels. Next, divided proteins were transferred onto poly(vinylidene fluoride) (PVDF) membranes. After being blocked with QuickBlock blocking buffer (P0252, Beyotime Biotechnology, Shanghai, China), the membranes were immersed in the primary antibodies against Keap1 (ab227828, 1:2000, Abcam), SOD2 (ab68155, 1:1000, Abcam), Caspase-3 (9662, 1:1000, CST), Cyto C (ab133504, 1:5000), α-SMA (ab124964, 1:1000, Abcam), Col I (EPR7785, 1:1000, Abcam), KIM-1 (ab78494, 1:1000,abcam), GAPDH (2118, 1:1000, CST), and β-Actin (4970, 1:1000, CST) at 4 °C overnight. After treatment with secondary antibodies, membranes were exposed by the ChemiDoc Touch imaging system (Bio-Rad).

Transmission Electron Microscopy. Renal tissues were fixed in 2.5% glutaraldehyde, followed by 1% osmium tetroxide fixation, dehydration in a series of alcohols, and embedded in epoxy resin. TEM examination of ultrathin slices stained using uranyl acetate and lead citrate (JEM-1400plus).

Immunohistochemistry Staining. The harvested kidney tissues were fixed and then embedded. Sliced kidney tissue was treated with primary antibodies against SOD2 (ab68155, Abcam) and Keap1 (ab227828, Abcam) and subsequently added with the secondary antibody. Images were scanned using a slide scanner (3DHISTECH), and IHC scores were analyzed using ImageJ with plugin IHC profiler. The formula used to count scores is as below:[76]

$$\text{score} = \frac{(\text{number of pixels in a zone}) \times (\text{score of the zone})}{\text{total number of pixels in the image}}$$

Immunofluorescence Staining. Immunofluorescence staining was applied to obtain the mechanism at the protein level. After treatment as described above, the cells were fixed with 4% cold paraformaldehyde, permeabilized with 0.5% Triton X-100, and blocked with 5% goat serum. After PBS washing, the samples were incubated with primary antibodies against Keap1 (ab227828, 1:500, Abcam), SOD2 (ab110300, 1:300, Abcam), Caspase-3 (ab32351, 1:500, Abcam), Cyto C (ab133504, 1:100), α-SMA (ab124964, 1:500, Abcam), and Col I (EPR7785, 1:300, Abcam) overnight at 4 °C. After rewashing them on the second day, cells were added with the secondary antibody (1:500) and stained with phalloidin and DAPI. Immunofluorescence images were obtained by confocal laser microscopy (FV3000, Olympus). Slices of kidney tissue were incubated with primary antibodies against KIM-1(ab78494, Abcam) and then with secondary antibodies. Stained samples were scanned by a slide scanner (3DHISTECH).

Safety Assay. In the heart, liver, spleen, and lung tissue sections, histological manifestations were displayed by H&E staining.

Statistical Analysis. Statistical analyses were accomplished with GraphPad Prism 9.4. Unpaired *t* test was used for comparison among groups and simple linear regression for linear correlation. Statistical analysis: *P*-value <0.05 was considered to be statistically significant. */#/@/& $P < 0.05$, **/##/@@/&& $P < 0.01$, ***/###/@@@/&&& $P < 0.001$ (*, control/Sham; #, I/R injury/AKI+saline; @, tFNAs/AKI+ tFNAs; &, Typ/AKI+Typ).

ASSOCIATED CONTENT

Supporting Information

The Supporting Information is available free of charge at https://pubs.acs.org/doi/10.1021/acsnano.3c02102.

Figures of standard curve of Typ and capsulation of Typ into tFNAs, stability of tFNA and TTC in 10% fetal bovine serum, cell viability of tFNAs and TTC in different concentrations, stability and biodistribution of tFNA and TTC *in vivo*, and histological changes in the

https://doi.org/10.1021/acsnano.3c02102
ACS Nano 2023, 17, 8767−8781

heart, liver, spleen, and lung and table of base sequences of the ssDNAs used to construct the tFNAs (PDF)

AUTHOR INFORMATION

Corresponding Author

Yunfeng Lin − *State Key Laboratory of Oral Diseases, National Clinical Research Centre for Oral Diseases, West China Hospital of Stomatology, Sichuan University, Chengdu 610041, P. R. China; Sichuan Provincial Engineering Research Center of Oral Biomaterials, Chengdu, Sichuan 610041, China;* orcid.org/0000-0003-1224-6561; Email: yunfenglin@scu.edu.cn

Authors

Ran Yan − *State Key Laboratory of Oral Diseases, National Clinical Research Centre for Oral Diseases, West China Hospital of Stomatology, Sichuan University, Chengdu 610041, P. R. China; Sichuan Provincial Engineering Research Center of Oral Biomaterials, Chengdu, Sichuan 610041, China*

Weitong Cui − *State Key Laboratory of Oral Diseases, National Clinical Research Centre for Oral Diseases, West China Hospital of Stomatology, Sichuan University, Chengdu 610041, P. R. China; Sichuan Provincial Engineering Research Center of Oral Biomaterials, Chengdu, Sichuan 610041, China*

Wenjuan Ma − *State Key Laboratory of Oral Diseases, National Clinical Research Centre for Oral Diseases, West China Hospital of Stomatology, Sichuan University, Chengdu 610041, P. R. China; Sichuan Provincial Engineering Research Center of Oral Biomaterials, Chengdu, Sichuan 610041, China*

Jiajie Li − *State Key Laboratory of Oral Diseases, National Clinical Research Centre for Oral Diseases, West China Hospital of Stomatology, Sichuan University, Chengdu 610041, P. R. China; Sichuan Provincial Engineering Research Center of Oral Biomaterials, Chengdu, Sichuan 610041, China*

Zhiqiang Liu − *State Key Laboratory of Oral Diseases, National Clinical Research Centre for Oral Diseases, West China Hospital of Stomatology, Sichuan University, Chengdu 610041, P. R. China; Sichuan Provincial Engineering Research Center of Oral Biomaterials, Chengdu, Sichuan 610041, China*

Complete contact information is available at: https://pubs.acs.org/10.1021/acsnano.3c02102

Notes

The authors declare no competing financial interest.

ACKNOWLEDGMENTS

All animal surgeries were carried out following the Use Guide of Experimental Animal Care of Sichuan University and approved by the Ethics Committee of the State Key Laboratory of Oral Disease Research of Sichuan University. This study was supported by the National Key R&D Program of China (2019YFA0110600) and the National Natural Science Foundation of China (81970916 and 81671031). Thanks to Dr. Yun Wang for the histological scoring.

REFERENCES

(1) Science Direct.. Section 2: AKI Definition. *Kidney Int. Suppl.* **2011**, *2* (1), 19−36.

(2) Bellomo, R.; Kellum, J. A.; Ronco, C. Acute Kidney Injury. *Lancet* **2012**, *380* (9843), 756−66.

(3) Bellomo, R.; Ronco, C.; Kellum, J. A.; Mehta, R. L.; Palevsky, P. Acute Dialysis Quality Initiative, w. Acute Renal Failure - Definition, Outcome Measures, Animal Models, Fluid Therapy and Information Technology Needs: the Second International Consensus Conference of the Acute Dialysis Quality Initiative (ADQI) Group. *Crit Care* **2004**, *8* (4), R204−12.

(4) Ostermann, M.; Bellomo, R.; Burdmann, E. A.; Doi, K.; Endre, Z. H.; Goldstein, S. L.; Kane-Gill, S. L.; Liu, K. D.; Prowle, J. R.; Shaw, A. D.; Srisawat, N.; Cheung, M.; Jadoul, M.; Winkelmayer, W. C.; Kellum, J. A.; Conference, P. Controversies in Acute Kidney Injury: Conclusions from a Kidney Disease: Improving Global Outcomes (KDIGO) Conference. *Kidney Int.* **2020**, *98* (2), 294−309.

(5) Li, P. K. T.; Burdmann, E. A.; Mehta, R. L. Acute Kidney Injury: Global Health Alert. *Kidney Int.* **2013**, *83* (3), 372−376.

(6) Rewa, O.; Bagshaw, S. M. Acute Kidney Injury-Epidemiology, Outcomes and Economics. *Nat. Rev. Nephrol* **2014**, *10* (4), 193−207.

(7) Hoste, E. A. J.; Kellum, J. A.; Selby, N. M.; Zarbock, A.; Palevsky, P. M.; Bagshaw, S. M.; Goldstein, S. L.; Cerda, J.; Chawla, L. S. Global Epidemiology and Outcomes of Acute Kidney Injury. *Nat. Rev. Nephrol* **2018**, *14* (10), 607−625.

(8) Mehta, R. L.; Kellum, J. A.; Shah, S. V.; Molitoris, B. A.; Ronco, C.; Warnock, D. G.; Levin, A. Acute Kidney Injury, N. Acute Kidney Injury Network: Report of an Initiative to Improve Outcomes in Acute Kidney Injury. *Crit Care* **2007**, *11* (2), R31.

(9) Schrier, R. W. Early Intervention in Acute Kidney Injury. *Nat. Rev. Nephrol* **2010**, *6* (1), 56−9.

(10) Leung, K. C.; Tonelli, M.; James, M. T. Chronic Kidney Disease Following Acute Kidney Injury-Risk and Outcomes. *Nat. Rev. Nephrol* **2013**, *9* (2), 77−85.

(11) James, M. T.; Bhatt, M.; Pannu, N.; Tonelli, M. Long-Term Outcomes of Acute Kidney Injury and Strategies for Improved Care. *Nat. Rev. Nephrol* **2020**, *16* (4), 193−205.

(12) Hoste, E. A.; De Loor, J. Acute kidney injury: Zero Deaths From AKI by 2025: Focus on Awareness and Therapy. *Nat. Rev. Nephrol* **2016**, *12* (7), 379−80.

(13) Kellum, J. A.; Romagnani, P.; Ashuntantang, G.; Ronco, C.; Zarbock, A.; Anders, H. J. Acute Kidney Injury. *Nat. Rev. Dis. Primers* **2021**, *7* (1), 52.

(14) Scholz, H.; Boivin, F. J.; Schmidt-Ott, K. M.; Bachmann, S.; Eckardt, K. U.; Scholl, U. I.; Persson, P. B. Kidney Physiology and Susceptibility to Acute Kidney Injury: Implications for Renoprotection. *Nat. Rev. Nephrol* **2021**, *17* (5), 335−349.

(15) Ferenbach, D. A.; Bonventre, J. V. Mechanisms of Maladaptive Repair after AKI Leading to Accelerated Kidney Ageing and CKD. *Nat. Rev. Nephrol* **2015**, *11* (5), 264−76.

(16) Messerer, D. A. C.; Halbgebauer, R.; Nilsson, B.; Pavenstadt, H.; Radermacher, P.; Huber-Lang, M. Immunopathophysiology of Trauma-Related Acute Kidney Injury. *Nat. Rev. Nephrol* **2021**, *17* (2), 91−111.

(17) Emma, F.; Montini, G.; Parikh, S. M.; Salviati, L. Mitochondrial Dysfunction in Inherited Renal Disease and Acute Kidney Injury. *Nat. Rev. Nephrol* **2016**, *12* (5), 267−80.

(18) Bhargava, P.; Schnellmann, R. G. Mitochondrial Energetics in the Kidney. *Nat. Rev. Nephrol* **2017**, *13* (10), 629−646.

(19) Tang, C.; Cai, J.; Yin, X. M.; Weinberg, J. M.; Venkatachalam, M. A.; Dong, Z. Mitochondrial Quality Control in Kidney Injury and Repair. *Nat. Rev. Nephrol* **2021**, *17* (5), 299−318.

(20) Cox, C. S.; McKay, S. E.; Holmbeck, M. A.; Christian, B. E.; Scortea, A. C.; Tsay, A. J.; Newman, L. E.; Shadel, G. S. Mitohormesis in Mice *via* Sustained Basal Activation of Mitochondrial and Antioxidant Signaling. *Cell Metab.* **2018**, *28* (5), 776−786.

(21) Forbes, J. M.; Thorburn, D. R. Mitochondrial Dysfunction in Diabetic Kidney Disease. *Nat. Rev. Nephrol* **2018**, *14* (5), 291−312.

(22) Chen, P.; Cao, Y.; Bao, B.; Zhang, L.; Ding, A. Antioxidant Capacity of Typha Angustifolia Extracts and Two Active Flavonoids. *Pharm. Biol.* **2017**, *55* (1), 1283−1288.
(23) Su, S.; Hua, Y.; Duan, J. A.; Zhou, W.; Shang, E.; Tang, Y. Inhibitory Effects of Active Fraction and its Main Components of Shaofu Zhuyu Decoction on Uterus Contraction. *Am. J. Chin Med.* **2010**, *38* (4), 777−87.
(24) Chen, P.; Liu, S.; Dai, G.; Xie, L.; Xu, J.; Zhou, L.; Ju, W.; Ding, A. Determination of Typhaneoside in Rat Plasma by Liquid Chromatography-Tandem Mass Spectrometry. *J. Pharm. Biomed Anal* **2012**, *70*, 636−9.
(25) Su, S. L.; Yu, L.; Hua, Y. Q.; Duan, J. A.; Deng, H. S.; Tang, Y. P.; Lu, Y.; Ding, A. W. Screening and Analyzing the Potential Bioactive Components from Shaofu Zhuyu Decoction, Using Human Umbilical Vein Endothelial Cell Extraction and High-Performance Liquid Chromatography Coupled with Mass Spectrometry. *Biomed Chromatogr* **2008**, *22* (12), 1385−92.
(26) Huang, X.; Su, S.; Cui, W.; Liu, P.; Duan, J. A.; Guo, J.; Li, Z.; Shang, E.; Qian, D.; Huang, Z. Simultaneous Determination of Paeoniflorin, Albiflorin, Ferulic Acid, Tetrahydropalmatine, Protopine, Typhaneoside, Senkyunolide I in Beagle Dogs Plasma by UPLC-MS/MS and Its Ppplication to a Pharmacokinetic Study after Oral Administration of Shaofu Zhuyu Decoction. *J. Chromatogr B Analyt Technol. Biomed Life Sci.* **2014**, *962*, 75−81.
(27) Liu, J. Y.; Yu, H. S.; Feng, B.; Kang, L. P.; Pang, X.; Xiong, C. Q.; Zhao, Y.; Li, C. M.; Zhang, Y.; Ma, B. P. Selective Hydrolysis of Flavonoid Glycosides by Curvularia Lunata. *Chin J. Nat. Med.* **2013**, *11* (6), 684−9.
(28) Zhu, H. Y.; Huang, Z. X.; Chen, G. Q.; Sheng, F.; Zheng, Y. S. Typhaneoside Prevents Acute Myeloid Leukemia (AML) Through Suppressing Proliferation and Inducing Ferroptosis Associated with Autophagy. *Biochem. Biophys. Res. Commun.* **2019**, *516* (4), 1265−1271.
(29) Barboza, J. R.; Pereira, F. A. N.; Fernandes, R. A.; Vasconcelos, C. C.; Cartagenes, M.; Oliveira Lopes, A. J.; Melo, A. C.; Guimaraes, I. D. S.; Rocha, C. Q. D.; Ribeiro, M. N. S. Cytotoxicity and Pro-Apoptotic, Antioxidant and Anti-Inflammatory Activities of Geopropolis Produced by the Stingless Bee Melipona Fasciculata Smith. *Biology (Basel).* **2020**, *9* (9), 292.
(30) Tang, J.-L.; Liu, B.-Y.; Ma, K.-W. Traditional Chinese Medicine. *Lancet* **2008**, *372* (9654), 1938−1940.
(31) Xue, T. Synergy in Traditional Chinese Medicine. *Lancet Oncol* **2016**, *17* (2), No. e39.
(32) Wang, X.; Chen, X.; Li, J.; Evans, O. B.; Wang, H.; Yang, X.; He, J.; Gao, X. M.; Chang, Y. X. Thrombin-Based Discovery Strategy of Bioactive-Chemical Quality Marker Combination for Pollen of Typha Orientalis by Metabolomics Coupled with Chemometrics. *Phytomedicine* **2020**, *75*, 153246.
(33) Songhang, L.; Yuhao, L.; Tao, Z.; Shiyu, L.; Sirong, S.; Jiajun, H.; Yu, X.; Xiaoxiao, C.; Taoran, T.; Yunfeng, L. A Tetrahedral Framework DNA-based Bioswitchable MiRNA Inhibitor Delivery System: Application to Skin Anti-Aging. *Adv. Mater.* **2022**, *34* (46), No. 2204287.
(34) Zhang, M.; Zhang, X.; Tian, T.; Zhang, Q.; Wen, Y.; Zhu, J.; Xiao, D.; Cui, W.; Lin, Y. Anti-Inflammatory Activity of Curcumin-Loaded Tetrahedral Framework Nucleic Acids on Acute Gouty Arthritis. *Bioact Mater.* **2022**, *8*, 368−380.
(35) Zhang, B.; Tian, T.; Xiao, D.; Gao, S.; Cai, X.; Lin, Y. Facilitating *In Situ* Tumor Imaging with a Tetrahedral DNA Framework-Enhanced Hybridization Chain Reaction Probe. *Adv. Funct. Mater.* **2022**, *32* (16), 2109728.
(36) Ji, X.; Li, Q.; Song, H.; Fan, C. Protein-Mimicking Nanoparticles in Biosystems. *Adv. Mater.* **2022**, *34* (37), No. 2201562.
(37) Zhang, T.; Tian, T.; Lin, Y. Functionalizing Framework Nucleic-Acid-Based Nanostructures for Biomedical Application. *Adv. Mater.* **2022**, *34* (46), No. 2107820.
(38) Ma, W.; Yang, Y.; Zhu, J.; Jia, W.; Zhang, T.; Liu, Z.; Chen, X.; Lin, Y. Biomimetic Nanoerythrosome-Coated Aptamer-DNA Tetrahedron/Maytansine Conjugates: pH-Responsive and Targeted Cytotoxicity for HER2-Positive Breast Cancer. *Adv. Mater.* **2022**, *34* (46), No. 2109609.
(39) Zhu, J.; Yang, Y.; Ma, W.; Wang, Y.; Chen, L.; Xiong, H.; Yin, C.; He, Z.; Fu, W.; Xu, R.; Lin, Y. Antiepilepticus Effects of Tetrahedral Framework Nucleic Acid *via* Inhibition of Gliosis-Induced Downregulation of Glutamine Synthetase and Increased AMPAR Internalization in the Postsynaptic Membrane. *Nano Lett.* **2022**, *22* (6), 2381−2390.
(40) Li, J.; Yao, Y.; Wang, Y.; Xu, J.; Zhao, D.; Liu, M.; Shi, S.; Lin, Y. Modulation of the Crosstalk between Schwann Cells and Macrophages for Nerve Regeneration: A Therapeutic Strategy Based on a Multifunctional Tetrahedral Framework Nucleic Acids System. *Adv. Mater.* **2022**, *34* (46), No. 2270320.
(41) Gao, Y.; Chen, X.; Tian, T.; Zhang, T.; Gao, S.; Zhang, X.; Yao, Y.; Lin, Y.; Cai, X. A Lysosome-Activated Tetrahedral Nanobox for Encapsulated siRNA Delivery. *Adv. Mater.* **2022**, *34* (46), No. 2201731.
(42) Qin, X.; Xiao, L.; Li, N.; Hou, C.; Li, W.; Li, J.; Yan, N.; Lin, Y. Tetrahedral Framework Nucleic Acids-based Delivery of MicroRNA-155 Inhibits Choroidal Neovascularization by Regulating the Polarization of Macrophages. *Bioact Mater.* **2022**, *14*, 134−144.
(43) Zhou, M.; Zhang, T.; Zhang, B.; Zhang, X.; Gao, S.; Zhang, T.; Li, S.; Cai, X.; Lin, Y. A DNA Nanostructure-Based Neuroprotectant against Neuronal Apoptosis *via* Inhibiting Toll-like Receptor 2 Signaling Pathway in Acute Ischemic Stroke. *ACS Nano* **2022**, *16* (1), 1456−1470.
(44) Wang, Y.; Li, Y.; Gao, S.; Yu, X.; Chen, Y.; Lin, Y. Tetrahedral Framework Nucleic Acids Can Alleviate Taurocholate-Induced Severe Acute Pancreatitis and Its Subsequent Multiorgan Injury in Mice. *Nano Lett.* **2022**, *22* (4), 1759−1768.
(45) Li, J.; Lai, Y.; Li, M.; Chen, X.; Zhou, M.; Wang, W.; Li, J.; Cui, W.; Zhang, G.; Wang, K.; Liu, L.; Lin, Y. Repair of Infected Bone Defect with Clindamycin-Tetrahedral DNA Nanostructure Complex-Loaded 3D Bioprinted Hybrid Scaffold. *Chem. Eng. J.* **2022**, *435*, 134855.
(46) Zhang, Q.; Lin, S.; Wang, L.; Peng, S.; Tian, T.; Li, S.; Xiao, J.; Lin, Y. Tetrahedral Framework Nucleic Acids Act as Antioxidants in Acute Kidney Injury Treatment. *Chem. Eng. J.* **2021**, *413*, 127426.
(47) Crisafuli, F. A.; Ramos, E. B.; Rocha, M. S. Characterizing the Interaction between DNA and GelRed Fluorescent Stain. *Eur. Biophys J.* **2015**, *44* (1−2), 1−7.
(48) Zhang, T.; Zhou, M.; Xiao, D.; Liu, Z.; Jiang, Y.; Feng, M.; Lin, Y.; Cai, X. Myelosuppression Alleviation and Hematopoietic Regeneration by Tetrahedral-Framework Nucleic-Acid Nanostructures Functionalized with Osteogenic Growth Peptide. *Adv. Sci.* **2022**, *9* (27), 2202058.
(49) Liu, Z.; Chen, X.; Ma, W.; Gao, Y.; Yao, Y.; Li, J.; Zhang, T.; Qin, X.; Ge, Y.; Jiang, Y.; Lin, Y. Suppression of Lipopolysaccharide-Induced Sepsis by Tetrahedral Framework Nucleic Acid Loaded with Quercetin. *Adv. Funct. Mater.* **2022**, *32* (43), 2204587.
(50) Manford, A. G.; Rodríguez-Pérez, F.; Shih, K. Y.; Shi, Z.; Berdan, C. A.; Choe, M.; Titov, D. V.; Nomura, D. K.; Rape, M. A Cellular Mechanism to Detect and Alleviate Reductive Stress. *Cell* **2020**, *183* (1), 46−61.
(51) Zhong, X.; Cui, P.; Cai, Y.; Wang, L.; He, X.; Long, P.; Lu, K.; Yan, R.; Zhang, Y.; Pan, X.; Zhao, X.; Li, W.; Zhang, H.; Zhou, Q.; Gao, P. Mitochondrial Dynamics Is Critical for the Full Pluripotency and Embryonic Developmental Potential of Pluripotent Stem Cells. *Cell Metab.* **2019**, *29* (4), 979−992.
(52) Lefebvre, A.; Ma, D.; Kessenbrock, K.; Lawson, D. A.; Digman, M. A. Automated Segmentation and Tracking of Mitochondria in Live-Cell Time-Lapse Images. *Nat. Methods* **2021**, *18* (9), 1091−1102.
(53) Katoh, I.; Sato, S.; Fukunishi, N.; Yoshida, H.; Imai, T.; Kurata, S. Apaf-1-Deficient Fog Mouse Cell Apoptosis Involves Hypo-Polarization of the Mitochondrial Inner Membrane, ATP Depletion and Citrate Accumulation. *Cell Res.* **2008**, *18* (12), 1210−9.

https://doi.org/10.1021/acsnano.3c02102
ACS Nano 2023, 17, 8767−8781

(54) Guo, C.; Dong, G.; Liang, X.; Dong, Z. Epigenetic Regulation in AKI and Kidney Repair: Mechanisms and Therapeutic Implications. *Nat. Rev. Nephrol* **2019**, *15* (4), 220−239.
(55) Choi, M. E. Autophagy in Kidney Disease. *Annu. Rev. Physiol.* **2020**, *82*, 297−322.
(56) Ruiz-Ortega, M.; Rayego-Mateos, S.; Lamas, S.; Ortiz, A.; Rodrigues-Diez, R. R. Targeting the Progression of Chronic Kidney Disease. *Nat. Rev. Nephrol* **2020**, *16* (5), 269−288.
(57) Birkelo, B. C.; Pannu, N.; Siew, E. D. Overview of diagnostic criteria and epidemiology of acute kidney injury and acute kidney disease in the critically ill patient. *Clin. J. Am. Soc. Nephrol.* **2022**, *17*, 717−735.
(58) Peerapornratana, S.; Manrique-Caballero, C. L.; Gómez, H.; Kellum, J. A. Acute kidney injury from sepsis: current concepts, epidemiology, pathophysiology, prevention and treatment. *Kidney Int.* **2019**, *96*, 1083−1099.
(59) Ostermann, M.; Lumlertgul, N.; Wilson, F. P. Predictive Models for Acute Kidney Injury Following Cardiac Surgery: The Importance of Accurate and Actionable Prediction. *JAMA* **2022**, *327* (10), 927−929.
(60) Demirjian, S.; Bashour, C. A.; Shaw, A.; Schold, J. D.; Simon, J.; Anthony, D.; Soltesz, E.; Gadegbeku, C. A. Predictive Accuracy of a Perioperative Laboratory Test-Based Prediction Model for Moderate to Severe Acute Kidney Injury After Cardiac Surgery. *JAMA* **2022**, *327* (10), 956−964.
(61) Morioka, S.; Kajioka, D.; Yamaoka, Y.; Ellison, R. M.; Tufan, T.; Werkman, I. L.; Tanaka, S.; Barron, B.; Ito, S. T.; Kucenas, S.; Okusa, M. D.; Ravichandran, K. S. Chimeric efferocytic receptors improve apoptotic cell clearance and alleviate inflammation. *Cell* **2022**, *185* (26), 4887−4903.
(62) Verstovsek, S.; Gerds, A. T.; Vannucchi, A. M.; Al-Ali, H. K.; Lavie, D.; Kuykendall, A. T.; Grosicki, S.; Iurlo, A.; Goh, Y. T.; Lazaroiu, M. C.; Egyed, M.; Fox, M. L.; McLornan, D.; Perkins, A.; Yoon, S. S.; Gupta, V.; Kiladjian, J. J.; Granacher, N.; Lee, S. E.; Ocroteala, L.; Passamonti, F.; Harrison, C. N.; Klencke, B. J.; Ro, S.; Donahue, R.; Kawashima, J.; Mesa, R. MOMENTUM Study Investigators. Momelotinib versus danazol in symptomatic patients with anaemia and myelofibrosis (MOMENTUM): results from an international, double-blind, randomised, controlled, phase 3 study. *Lancet* **2023**, *401* (10373), 269−280.
(63) Lee, C. D.; Hinson, J.; Davenport, M. S. Avoiding Contrast-Enhanced Imaging to Prevent Contrast-Induced Acute Kidney Injury. *N Engl J. Med.* **2022**, *387* (19), 1809−1812.
(64) James, M. T.; Har, B. J.; Tyrrell, B. D.; Faris, P. D.; Tan, Z.; Spertus, J. A.; Wilton, S. B.; Ghali, W. A.; Knudtson, M. L.; Sajobi, T. T.; Pannu, N. I.; Klarenbach, S. W.; Graham, M. M. Effect of Clinical Decision Support with Audit and Feedback on Prevention of Acute Kidney Injury in Patients Undergoing Coronary Angiography: A Randomized Clinical Trial. *JAMA* **2022**, *328* (9), 839−849.
(65) Noone, D. G.; Iijima, K.; Parekh, R. Idiopathic nephrotic syndrome in children. *Lancet* **2018**, *392* (10141), 61−74.
(66) Cowan, A. J.; Green, D. J.; Kwok, M.; Lee, S.; Coffey, D. G.; Holmberg, L. A.; Tuazon, S.; Gopal, A. K.; Libby, E. N. Diagnosis and Management of Multiple Myeloma: A Review. *JAMA* **2022**, *327* (5), 464−477.
(67) Messerer, D. A. C.; Halbgebauer, R.; Nilsson, B.; Pavenstädt, H.; Radermacher, P.; Huber-Lang, M. Immunopathophysiology of trauma-related acute kidney injury. *Nat. Rev. Nephrol* **2021**, *17* (2), 91−111.
(68) Simonetto, D. A.; Gines, P.; Kamath, P. S. Hepatorenal syndrome: pathophysiology, diagnosis, and management. *BMJ.* **2020**, *370*, m2687.
(69) Murphy, E.; Steenbergen, C. Mechanisms underlying acute protection from cardiac ischemia-reperfusion injury. *Physiol Rev.* **2008**, *88* (2), 581−609.
(70) Eltzschig, H. K.; Eckle, T. Ischemia and reperfusion–from mechanism to translation. *Nat. Med.* **2011**, *17* (11), 1391−401.
(71) Ganote, C. E.; Worstell, J.; Kaltenbach, J. P. Oxygen-induced enzyme release after irreversible myocardial injury. Effects of cyanide in perfused rat hearts. *Am. J. Pathol.* **1976**, *84* (2), 327−350.
(72) Loor, G.; Kondapalli, J.; Iwase, H.; Chandel, N. S.; Waypa, G. B.; Guzy, R. D.; Vanden Hoek, T. L.; Schumacker, P. T. Mitochondrial oxidant stress triggers cell death insimulated ischemia-reperfusion. *Biochim. Biophys. Acta* **2011**, *1813* (7), 1382−1394.
(73) Kolbrink, B.; von, F. A.; Murphy, J. M.; Krautwald, S. Role of necroptosis in kidney health and disease. *Nat. Rev. Nephrol.* **2023**, *19*, 300−314.
(74) Pillai, R.; Hayashi, M.; Zavitsanou, A.-M.; Papagiannakopoulos, T. NRF2: KEAPing Tumors Protected. *Cancer Discov.* **2022**, *12*, 625−643.
(75) Zhang, D. D.; Lo, S. C.; Cross, J. V.; Templeton, D. J.; Hannink, M. Keap1 is a redox-regulated substrate adaptor protein for a Cul3-dependent ubiquitin ligase complex. *Molecular and cellular biology* **2004**, *24* (24), 10941−10953.
(76) Varghese, F.; Bukhari, A. B.; Malhotra, R.; De, A. IHC Profiler: An Open Source Plugin for the Quantitative Evaluation and Automated Scoring of Immunohistochemistry Images of Human Tissue Samples. *PLoS One* **2014**, *9* (5), No. e96801.

https://doi.org/10.1021/acsnano.3c02102
ACS Nano 2023, 17, 8767−8781